

See discussions, stats, and author profiles for this publication at: <https://www.researchgate.net/publication/281483927>

Role of the Chemically Non-Innocent Ligand in the Catalytic Formation of Hydrogen and Carbon Dioxide from Methanol and Water with the Metal as the Spectator

ARTICLE *in* JOURNAL OF THE AMERICAN CHEMICAL SOCIETY · AUGUST 2015

Impact Factor: 12.11 · DOI: 10.1021/jacs.5b07444 · Source: PubMed

READS

53

2 AUTHORS:



Haixia Li

Texas A&M University

25 PUBLICATIONS 548 CITATIONS

[SEE PROFILE](#)



Michael B Hall

Texas A&M University

359 PUBLICATIONS 10,268 CITATIONS

[SEE PROFILE](#)

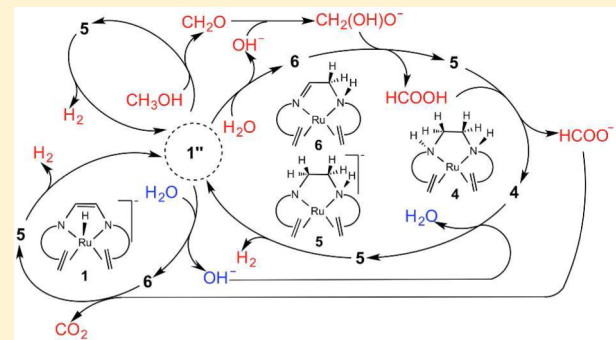
Role of the Chemically Non-Innocent Ligand in the Catalytic Formation of Hydrogen and Carbon Dioxide from Methanol and Water with the Metal as the Spectator

Haixia Li and Michael B. Hall*

Department of Chemistry, Texas A&M University, College Station, Texas 77843-3255, United States

Supporting Information

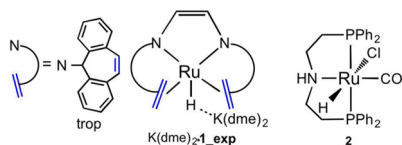
ABSTRACT: The catalytic mechanism for the production of H₂ and CO₂ from CH₃OH and H₂O by [K(dme)₂][Ru(H)(trop₂dad)] (K(dme)₂·1_exp) was investigated by density functional theory (DFT) calculations. Since the reaction occurs under mild conditions and at reasonable rates, it could be considered an ideal way to use methanol to store hydrogen. The predicted mechanism begins with the dehydrogenation of methanol to formaldehyde through a new ligand–ligand bifunctional mechanism, where two hydrogen atoms of CH₃OH eliminate to the ligand's N and C atoms, a mechanism that is more favorable than the previously known mechanisms, β-H elimination, or the metal–ligand bifunctional. The key initiator of this first step is formed by migration of the hydride in **1** from the ruthenium to the meta-carbon atom, which generates **1"** with a frustrated Lewis pair in the ring between N and C. Hydroxide, formed when **1"** cleaves H₂O, reacts rapidly with CH₂O to give H₂C(OH)O⁻, which subsequently donates a hydride to **6** to generate HCOOH and **5**. HCOOH then protonates **5** to give formate and a neutral complex, **4**, with a fully hydrogenated ligand. The hydride of formate transfers to **6**, releasing CO₂. The fully hydrogenated complex, **4**, is first deprotonated by OH⁻ to form **5**, which then releases hydrogen to regenerate the catalyst, **1"**. In this mechanism, which explains the experimental observations, the whole reaction occurs on the chemically non-innocent ligand with the ruthenium atom appearing as a spectator.



1. INTRODUCTION

Although hydrogen is an attractive “clean” energy carrier, as its combustion product is only water, its storage is still a challenge. Thus, the catalytic conversion of carbon dioxide and hydrogen to and from methanol and water (eq 1 in Chart 1) is considered

Chart 1



an ideal way to store and recover hydrogen because methanol contains ~12% hydrogen by weight and is a liquid at room temperature.¹ The conversion of methanol and water to carbon dioxide and 3 equiv of hydrogen is mildly endothermic by 9.3 kcal/mol (<http://cccbdb.nist.gov/hf0k.asp>). However, the conversion is generally realized by using methanol fuel cells (MFCs) or at high temperatures under heterogeneous catalysts with low efficiency.^{2,3} In contrast, homogeneous catalysts overcome these shortcomings and thus have potential

applications in energy storage. Furthermore, other uses of CO₂ to synthesize useful chemicals have been reviewed by several groups.⁴

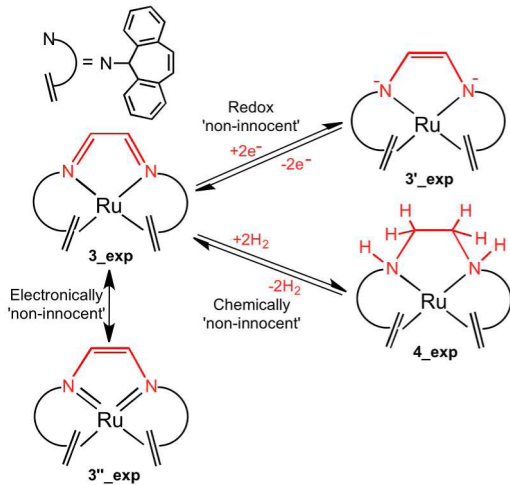
Several homogeneous catalysts for the conversion of methanol and water to carbon dioxide and hydrogen have been reported.⁵ In 2013, Grützmacher and co-workers synthesized the ruthenium complex [K(dme)₂][Ru(H)(trop₂dad)] (K(dme)₂·1_exp in Chart 1, trop₂dad = 1,4-bis(5H-dibenzo[*a,d*]cyclohepten-5-yl)-1,4-diazabuta-1,3-diene, and dme = dimethoxyethane).⁶ The complex was reported to catalyze the conversion of methanol and water to carbon dioxide and hydrogen with a high conversion (~80%). Remarkably, the reaction can occur at base-free conditions, representing a breakthrough in this area. Although Beller and co-workers also reported a base-free hydrogen generation from methanol, this involved a bicatalytic system. For the other examples, base is required. Among them, the mechanism for the ruthenium complex [RuHCl(CO) (HN(C₂H₄PPh₃)₂] (2 in Chart 1) has been investigated by density functional theory (DFT) calculations.⁸

In the literature, Grützmacher and co-workers proposed a mechanism for their reported catalytic reaction involving a

Received: July 16, 2015

neutral ruthenium complex $[\text{Ru}(\text{trop}_2\text{dad})]$ (**3_{exp}** in Chart 2) formed from the reaction of $\text{K}(\text{dme})_2 \cdot \mathbf{1}_{\text{exp}}$ and water with the

Chart 2



release of H_2 and OH^- .⁶ Complicating the nature of the species involved in this reaction is the non-innocent trop₂dad ligand,^{9,10} which can be redox “non-innocent” due to the transformation between trop-N=CH-CH=N-trop and trop-N⁻-CH=CH-N⁻-trop (for example, the transformation between **3_{exp}** and **3'_exp** in Chart 2)^{11,12} and chemically “non-innocent” with the formation of trop-NH-CH₂-CH₂-NH-trop by adding hydrogen atoms (for example, the transformation between **3_{exp}** and **4_{exp}**).¹³ Moreover, the trop₂dad ligand can also be electronically “non-innocent” due to its two resonance structures **3_{exp}** and **3''_{exp}** (Chart 2). Our following investigations on the mechanism show that the trop₂dad behaves like a chemically “non-innocent” ligand in the catalysis. In addition, although the olefinic groups of the trop residues are usually deemed to be just additional donor sites to help create a tetrachelating ligand, they may also act as “non-innocent” ligands. The “non-innocent” nature of alkene ligands in paramagnetic rhodium and iridium alkene complexes has been reported, and the “non-innocent” character is attributed to spin delocalization over the metal and the alkene ligand.¹⁴

Understanding the details of a catalytic mechanism may help researchers develop new catalysts or improve ones for known reactions. Herein, we investigated the complicated electronic structure and reactions of these ruthenium complexes by DFT calculations. In addition to calculating the mechanism proposed in the literature, which employs the neutral ruthenium complex, we also computed alternative pathways based on the anionic ruthenium complex.

2. COMPUTATIONAL DETAILS

The counterion $\text{K}(\text{dme})_2^+$ in the $\text{K}(\text{dme})_2 \cdot \mathbf{1}_{\text{exp}}$ complex is assumed to be a spectator cation for the anionic species **1_{exp}** and thus not involved in the reaction paths in these calculations. The “_{exp}” suffix is used to indicate the species with the full ligands. To investigate a variety of possible reaction pathways, we simplified the species **1_{exp}** as **1** by “cutting” the phenyl rings of the trop ligands and replacing the outer C_4H_4 groups with two H atoms (the simplified structures are shown in the following figures). This ligand simplification maintains the electronic structures and is considered reasonable for the initial explorations. Calculations with the full ligands are reported after these explorations.

To choose a reasonable basis set and functional, benchmark calculations were conducted on several model reactions. Seven basis sets and 33 DFT functionals were tested. The nonmetal atoms use the all-electron basis sets (BS), 6-31G(d),¹⁵ 6-31G(d,p),¹⁵ 6-311G(d,p),¹⁶ 6-311+G(d,p),¹⁷ and 6-311++G(d,p).¹⁷ The ruthenium metal atom uses the ECP-based BS including SDD,¹⁸ cc-pVTZ-PP,^{19,20} and AUG-cc-pVTZ-PP.^{19,20} The tested DFT functionals involve generalized gradient approximation (GGA), meta-GGA, global-hybrid GGA, global-hybrid meta-GGA, range-separate hybrid GGA, doubly hybrid methods, and functionals including dispersion. The details for the benchmark calculations are in the Supporting Information, SI1. According to the comparisons of various basis sets, single-point calculations at BS2, the combination of 6-311+G(d,p) and AUG-cc-pVTZ-PP, and at geometries optimized at the BS1, the combination of 6-31G(d) and SDD with the same functional, denoted by BS2//BS1, give the results close to that obtained from optimizations at BS2; thus, BS2//BS1 is employed in the test of DFT functionals. The single-point calculations with coupled cluster singles and doubles (CCSD)³⁰ and CCSD(T)³¹ were conducted at the BS3, the combination of 6-311+G(d,p) and cc-pVTZ-PP, at the geometries optimized at the level of ωB97XD /BS1. On the basis of the results of the four key reactions in SI1, the hybrid-meta-GGA M06 functional, which predicts results very close to those of CCSD(T) with an average error of less than 4 kcal/mol, was used in the calculations for this mechanistic study. Moreover, as a “double check”, the influence of functionals were examined by calculating the actual catalyst system with five functionals selected from SI1 involving meta-GGA M06L,²¹ long-range hybrid-GGA, ωB97XD ,²⁶ CAM-B3LYP,²⁷ OHSE2PBE, and MN12SX,²⁹ as ωB97XD and M06L were reported to perform well in calculating transition metal complexes,^{32,33} and the other three functionals also predict results comparable to those of CCSD and CCSD(T) in our preliminary calculations.

Geometries of all intermediates and transition states in the mechanistic study were optimized in gas phase at the level of M06/BS1. Harmonic vibrational frequencies were calculated to identify intermediates with no imaginary frequency and transition states with only one imaginary frequency. When necessary, IRC calculations³⁴ were conducted to verify that the transition states connected the reactants and products at the level of M06/BS1. The harmonic frequencies obtained after geometry optimizations were used for the thermal and entropic corrections for enthalpies and free energies at 298 K and 1 atm. In the experiment, the reaction was performed in a water-tetrahydrofuran (THF) mixture (water and THF are 40.0 and 30.8 mmol, respectively, as reported in the reaction b.3 of 3.1 in the Supporting Information of ref 6). Thus, on the basis of the optimized geometries in gas phase, the energetic results were further refined by single-point calculations with the SMD³⁵ solvent model using water or THF as solvent at the level of M06/BS2. An adjustment for the change in standard state from 1 atm to 1 M concentration of $RT \ln(24.5)$, 1.9 kcal/mol, was used for all the species in solution. For water itself in aqueous solution for which the standard state concentration is 55.6 M, an adjustment for the change from 1 to 55.6 M concentration of $RT \ln(55.6)$, 4.3 kcal/mol, was further employed (see SI2).³⁶ Solvation free energies were added to the free energies with the above adjustments for the change in standard state concentration and the enthalpies at the BS2. The free energies and enthalpies in water and the free energies in THF represented as $\Delta G_w[\Delta H_w](\Delta G_{\text{THF}})$ are reported here. Unless otherwise specified, the energies discussed in the text refer to the free energies in water. Some species in the calculations were found to have more than one structure, and the structure used here is the most favorable one. JIMP2 molecular visualizing and manipulating program was employed to draw all the three-dimensional molecular structures involved in this study.³⁷

All DFT calculations were performed using the Gaussian 09 programs,³⁸ and the CCSD and CCSD(T) calculations were conducted using the Molpro program.³⁹ The Natural Bond Orbital (NBO) analysis⁴⁰ was carried out at the M06/BS1 level to investigate the electronic structures of some species.

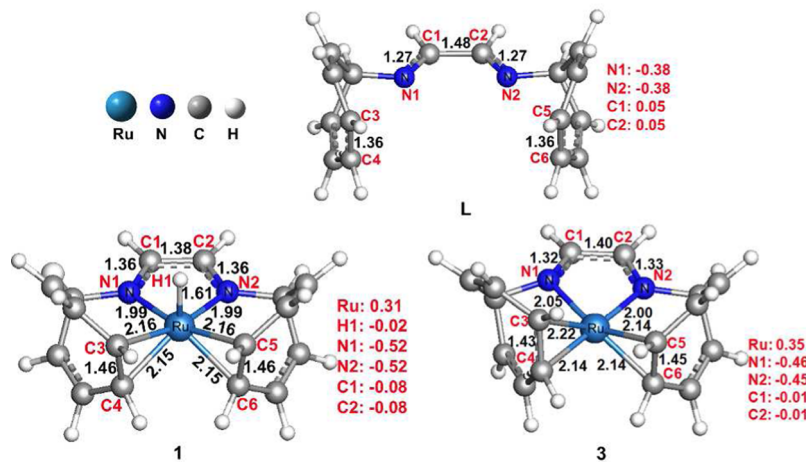


Figure 1. Optimized geometries for the free ligand L, the anionic species 1, and the neutral species 3. The black and red numbers are the selected bond lengths in Å and selected NPA charges. Selected bond distances (Å) of the X-ray structure of **1_{exp}**: Ru–N1:1.963(4), Ru–N2:1.978(4), Ru–H1:1.60(6), C3–C4:1.440(7), C5–C6:1.434(6), N1–C1:1.356(6), N2–C2:1.348(6), C1–C2:1.377(7).

3. RESULTS AND DISCUSSION

In the experimentally proposed mechanism, the anionic ruthenium complex **1_{exp}** first reacts with water to form the neutral ruthenium complex **3_{exp}** with the release of H₂ and OH⁻. The complex **3_{exp}** subsequently catalyzes the transformation of methanol and water to carbon dioxide and hydrogen. As mentioned in the **Introduction**, the trop₂dad ligands are considered to be non-innocent. Thus, the electronic structures of the species **1_{exp}** and **3_{exp}** were first analyzed in **section 3.1** by using their simplified models **1** and **3**. In addition, possible reaction mechanisms catalyzed by the anionic species **1** and the neutral species **3** were discussed therein; the former is found to be more favorable than the latter. The details for the catalytic steps with the anionic species **1** were reported in **section 3.2**. In **section 3.3**, selected transition states and intermediates of the actual catalyst, **1_{exp}**, were recalculated on the basis of the reported mechanism.

3.1. Electronic Structures of the Species 1 and 3. The anionic species **1** and the neutral species **3** are computed to be singlets; the corresponding triplet states are less stable by 18.4 and 8.5 kcal/mol, respectively. Unrestricted calculations of their open shell singlet diradicals repeatedly converged to the close shell singlet states. Optimized geometries and the natural population analysis (NPA) charges obtained from the NBO analysis are shown in **Figure 1**.

The neutral free ligand L is singlet and can be described as trop-N=CH–CH=N-trop on the basis of its optimized bond distances; for example, the C1=N1 and C2=N2 bonds are 1.27 Å, and the C1–C2 bond is 1.48 Å. In contrast, the ligand becomes trop-N⁻–CH=CH–N⁻–trop in the anionic ruthenium complex **1**, where the C1=N1 and C2=N2 bonds are 1.36 Å, and the C1=C2 bond is 1.38 Å. The NBO analysis for complex **1** (in **SI3**) is consistent with this description of the electronic structure, in which the doubly occupied p orbitals of two N atoms donate to the d orbitals of the ruthenium atom to form two partial Ru–N π bonds at 1.99 Å. Furthermore, the olefinic bond distances in the free ligand L (C3=C4 and C5=C6 at 1.36 Å) become much longer in the complex **1** (C3–C4 and C5–C6 at 1.46 Å), consistent with their crystal structures (C3–C4 at 1.440 Å and C5–C6 at 1.434 Å) and their experimental ¹H NMR spectrum.⁶ Thus, the trop fragment is supporting the π donation from N to Ru.

Unlike **1**, which has C_s symmetry, the optimized geometry of the neutral species **3** (**Figure 1**) has no symmetry; its C_{2v} and C_s structures are not local minima. In the species **3**, the C1–N1, C2–N2, and C1–C2 bonds have distances that are between those in the free ligand L and those in the species **1**, but like **1**, the C3–C4 and C5–C6 bond distances are long at 1.43 and 1.45 Å, respectively. The asymmetry mentioned above is most apparent here in the unexpected lengthening of Ru–C3 bond; the details of the unusual electronic structure and potential energy surface of **3** will be reported in the future.

In addition to reporting the catalytic reaction, Grützmacher and co-workers conducted several experiments to elucidate details of the mechanism. In one experiment, complex **4** was observed when adding EtOH and H₂O to a solution of **1**. In another experiment, **1** was regenerated from **4** when adding KO^tBu at 65 °C. Thus, on the basis of these experimental observations, they proposed a mechanism beginning with the neutral species **3** that was proposed to be generated from the reaction of **1** and H₂O with the release of H₂ and OH⁻. **3** reacts with methanol and water to produce the hydrogen-addition complex **4**, which then regenerates **1** by releasing H₂ and the proton to the base. However, our calculations predict that the production of the neutral species **3** from complex **4** is more unfavorable by over 24 kcal/mol in electronic energy than the formation of the anionic species **1** from complex **5** (Tables S4 and S5 in **SI1**). Moreover, the formation of **3**, H₂, and (OH⁻–H₂O)⁻ from the anionic species **1** and (H₂O⁻–H₂O) is computed to be endergonic by 0.3 and 16.4 kcal/mol in water and THF, respectively. As shown below, **section 3.2.2**, the highest barrier for the dehydrogenation of methanol, the first step in the whole catalytic reaction, is more than 30 kcal/mol for the neutral species **3**, which is higher than the barrier for the anionic species **1** (23.8 kcal/mol). Thus, a catalytic cycle based on the neutral species **3** seems less likely than one based on the anionic species **1**. Furthermore, the mechanism based on the anionic species **1** as discussed in the following explains these experimental observations.

3.2. Mechanism for the Catalytic Production of Carbon Dioxide and Hydrogen from Methanol and Water. The mechanism for the catalytic production of carbon dioxide and hydrogen (eq 1) by the anionic ruthenium complex **1** involves three steps: dehydrogenation of methanol to formaldehyde (step 1), hydroxide attack on formaldehyde

and formation of formate (step 2), and hydride transfer to release carbon dioxide and regenerate the catalyst (step 3). Formaldehyde was also proposed as a short-lived intermediate in the experiments.^{5,6,41,42} Likewise, both experimental and computational studies of the reduction of carbon dioxide to methanol by boranes or silanes were also reported to involve the formaldehyde intermediates.⁴³ The species **1''** that is formed from **1** through a hydrogen “walking” process, where the hydrogen atom migrates from the ruthenium atom in **1** to the nitrogen atom and then to the carbon atom, is considered an important species in the catalytic mechanism. Thus, the details for the hydrogen “walking” process are first discussed in section 3.2.1. Then the details for the three steps are described in the following sections 3.2.2, 3.2.3, and 3.2.4, respectively.

3.2.1. Hydrogen “Walking” Process. The calculated energy profiles for the hydrogen “walking” process are shown in Figure 2, and the optimized geometries for some species are in Figure

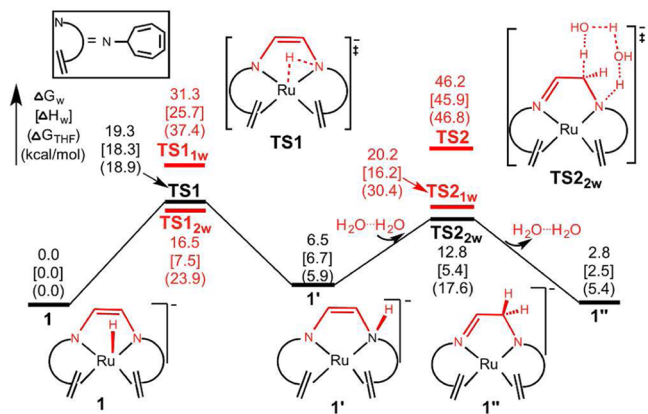


Figure 2. Energetic profiles for the formation of the species **1''** from the species **1** via the hydrogen “walking” process. Barriers for the two-water-mediated transition states **TS1_{2w}** and **TS2_{2w}** are relative to separated **1** and $(\text{H}_2\text{O}\cdots\text{H}_2\text{O})$.

3. As shown in Figure 2, the hydrogen first migrates from the ruthenium atom to the nitrogen atom over a barrier of 19.3 kcal/mol (**TS1**); this process generates a species **1'**. In the optimized geometry of **TS1**, the migrating hydrogen atom (H_1) becomes protonic (its net NPA charge is 0.22), while it is hydridic in the species **1** (its net NPA charge is -0.02) (see Figure 1). Likewise, the ruthenium atom in **TS1** is less positive than that in **1**. Water may assist this hydrogen migration process. However, the barrier for the one-water-mediated transition state **TS1_{1w}** is very high, 31.3 kcal/mol, relative to the separate reactants. Although the two-water-mediated transition state **TS1_{2w}** is close to **TS1** in free energy in water, **TS1_{2w}** is higher than **TS1** by 5.0 kcal/mol in THF. Thus, water does not seem to offer much help for this process. The intermediate species **1'** is at 6.5 kcal/mol relative to the species **1**. In the optimized geometry of **1'**, due to the protonation of the N_2 atom, the $\text{Ru}-\text{N}_2$ and C_2-N_2 bonds are longer than the $\text{Ru}-\text{N}_1$ and C_1-N_1 bonds. There is still a $\text{C}_1=\text{C}_2$ bond that has been confirmed by the NBO analysis (see SI3).

From species **1'**, the hydrogen atom moves from the nitrogen atom to the adjacent carbon atom to make the species **1''**. Two water molecules help this proton transfer process through transition state **TS2_{2w}**, where they act as proton shuttles. Relative to the separate reactants, **1** and $(\text{H}_2\text{O}\cdots\text{H}_2\text{O})$, the barrier for **TS2_{2w}** is only 12.8 kcal/mol, much lower than

those for the direct transition state **TS2** (46.2 kcal/mol) and one-water-mediated transition state **TS2_{1w}** (20.2 kcal/mol). Relative to the species **1**, the species **1''** formed after the proton transfer is at 2.8 kcal/mol. The optimized geometry of **1''** shows that it has a $\text{C}_1=\text{N}_1$ double bond at 1.28 Å and a C_1-C_2 single bond at 1.49 Å. The electronic structure of the species **1''** is verified by its NBO analysis results (see SI3). Further, complexes that are similar to species **1''** have been proposed as intermediates in other systems.⁴⁴

In addition to the hydrogen “walking” process shown in Figure 2, other possible pathways were studied (see SI4). These pathways involve the formation of **1''** from **1'** via the hydrogen migrating from the nitrogen atom to the meta-carbon atom and the formation of **1''** from **1** via the hydrogen migrating from the ruthenium to the carbon atom in one step. These pathways are less favorable than that in Figure 2. For example, the barriers for the formation of **1''** from **1** in one step without or with the aid of water are over 30 kcal/mol.

3.2.2. Dehydrogenation of Methanol to Formaldehyde. The β -H elimination transition state (TS) shown in Figure 4, panel A has been widely proposed for the dehydrogenation of alcohols by transition metal complexes.^{45–47} In this mechanism, the transition metal complex splits the alcohol’s O–H bond by using the metal alone or the metal–ligand active sites to generate the transition metal alkoxide complex. Subsequently, the H atom of the β -CHR₂ eliminates to the metal center through a four-member-ring transition state (Figure 4A), producing a transition metal hydride complex and the aldehyde. With non-innocent ligands, another β -H elimination TS in which the H atom of the β -CHR₂ eliminates to the non-innocent ligand rather than to the metal could occur (Figure 4B). Recently, a metal–ligand bifunctional TS, in which the alcohol’s proton (on the O atom) transfers to the non-innocent ligand and the alcohol’s H atom (on the β -C atom) transfers (as a hydride) to the transition metal atom, has been proposed (Figure 4C).⁴⁸ This mechanism may occur in a concerted or a stepwise fashion; generally in the latter, the proton transfers first and then the H^{0–} transfers. For some cases, the metal–ligand bifunctional mechanism has been calculated to be more favorable than the β -H elimination mechanism.⁴⁸ In this report, we propose a new bifunctional TS, a ligand–ligand bifunctional TS in which both H atoms from the alcohol (one on the O atom and the other on the β -C atom) transfer to the non-innocent ligand’s basic and acidic centers in a concerted or a stepwise fashion (Figure 4D).

By following the four TSs in Figure 4, possible pathways for the dehydrogenation of methanol with the anionic species **1**, **1'**, and **1''**, and the neutral species **3** were calculated. The most favorable among these possible pathways are shown in Figure 5. Other less favorable pathways shown in SI5 are discussed briefly below. As shown in Figure 5, once **1''** is generated, the CH₃OH’s proton and one H atom on the β -CH₃ move to the ligand’s N and sp² C atoms, respectively, by crossing a concerted ligand–ligand bifunctional transition state, **TS3**. Relative to separated **1** and methanol, the barrier for **TS3** is 23.8 kcal/mol, and the formed **5** after releasing CH₂O is at 11.3 kcal/mol. Both **Int1** and **Int2** are higher than their separated species; thus, no long-lived intermediates were formed before and after **TS3**. In the mechanism via **TS3**, the reaction occurs on the chemically non-innocent ligand with the Ru atom appearing as a spectator. Previously, bifunctional mechanisms occur on the Ru–N bond as the active site to accept the two H atoms of methanol by transferring the proton to the N and the H atom

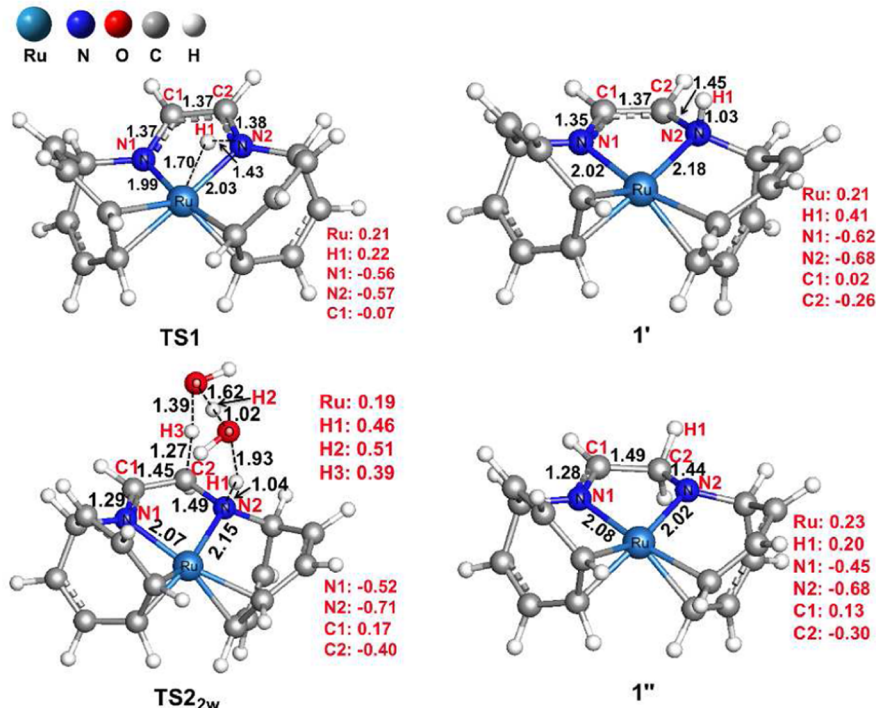


Figure 3. Optimized geometries of selected species involved in Figure 1. Geometries for the other species are in Figure S24 (SI15). The black and red numbers are selected bond lengths in Å and selected NPA charges, respectively.

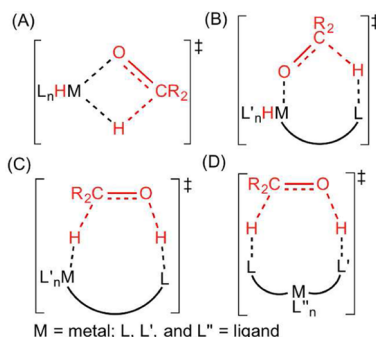


Figure 4. Proposed TSs for the dehydrogenation of alcohol (R_2CHOH , two R groups can be the same or different, or both can be H) by a transition metal complex. β -H elimination TSs, which follow the formation of the metal alkoxide complex, involve the H atom of the $\beta\text{-CH}_2$ eliminating to the metal (A) or to the ligand (B), while the bifunctional TSs, which transfer both H atoms of R_2CHOH (one on the O atom and the other on the $\beta\text{-C}$) in a concerted or a stepwise fashion, may be the metal–ligand bifunctional TS (C) or the ligand–ligand bifunctional TS (D).

on the $\beta\text{-CH}_3$ to the Ru atoms.^{8,49} However, such a mechanism is unfavorable in this system because the corresponding ruthenium hydride intermediates **5–3**, **5–5**, **5–9**, **5–10**, and **5–11** (the isomers of **5**) after releasing CH_2O are 37.4, 32.1, 54.7, 44.8, and 39.7 kcal/mol relative to separated **1** and methanol (see the Figure S2 in SI5). In a separate experiment conducted by Grüttmacher and co-workers, a complex with a deuterated trop₂dae ligand (trop₂dae is the fully hydrogenated trop₂dad) was observed by using the perdeuterated ethanol ($\text{CD}_3\text{CD}_2\text{OD}$) as a substrate.⁶ This observation supports the mechanism that the trop₂dad ligand of **1** participates in the dehydrogenation of alcohol.

The optimized geometry of **TS3** (Figure 6) corresponds to a concerted movement of the proton and H atom to the ligand, which was confirmed by an intrinsic reaction coordinate (IRC) analysis. The animation of the only one imaginary frequency of **TS3** also shows that both proton and H atom travel in the same direction, either away from or closer to the methanol. Furthermore, in following the IRC of **TS3**, the reactants complex (**Int1**) and the products complex (**Int2**) resulted from following the paths in the reverse and forward direction, respectively. The forming N–H bond in **TS3** is at 1.04 Å, which is close to that in the product **5**, while the forming C–H bond in **TS3** has a distance that is longer by 0.32 Å than the C–H bond in **5**. Thus, **TS3** is an asynchronous concerted transition state, where the proton transfers earlier than the H atom on the $\beta\text{-CH}_3$. The origin of this ligand-based reaction can be explained by a molecular orbital (MO) analysis (see the Scheme S1 and related discussions in SI5, page S33). The NPA charges of the active N and C atoms of **1''** are -0.68 and 0.13, respectively, in agreement with the fact that the proton and H atom transfer to the N and C atoms, respectively. Another transition state, where the proton and the H atom move in reverse sequence, that is, to C and N, respectively, would be considered less favorable due to the charge repulsions between them.

Other than the pathway via **TS3**, the next lowest energy pathway involves the formation of a neutral intermediate **6** and CH_3O^- from **1''** (or **1'**) and CH_3OH (the details are in the Figure S8 in SI5), followed by formation of **5** and CH_2O by crossing the rate-determining transition state, which is 1.7 kcal/mol less favorable than **TS3**. The two transition states were recalculated by using the full ligands, and the influence of functionals was further examined. According to the calculation results in the Table S7 in SI5, **TS3_exp** is still lower than this alternative.

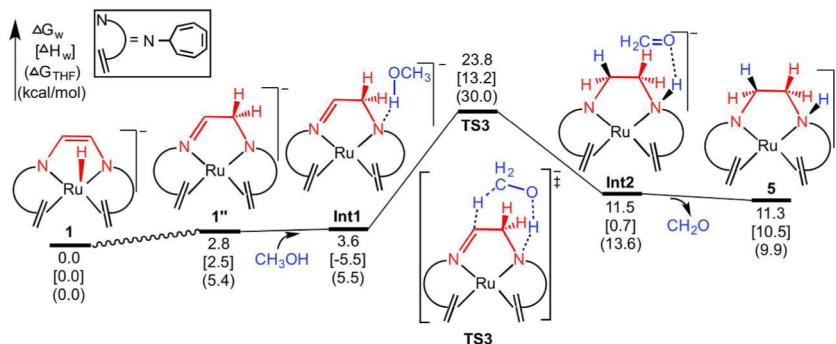


Figure 5. Energetic profiles for the dehydrogenation of methanol to formaldehyde.

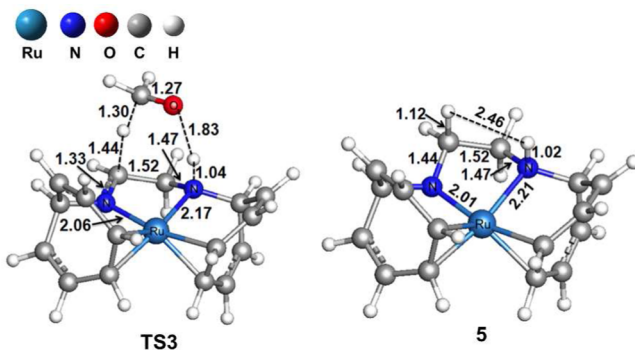


Figure 6. Optimized geometries for selected species in Figure 5. Geometries for the other species are in the Figure S25 in SI15. Selected bond lengths are in Å.

Because the originally proposed mechanism involves the ruthenium neutral complex 3 mediating the dehydrogenation of methanol,⁶ the four mechanisms in Figure 4 were recalculated

with the neutral complex 3 (see the Figures S10 and S11 in SI15). According to the results in Table S8 in SI15, the barriers for the methanol dehydrogenation transition states are over 30 kcal/mol relative to separated 3 and methanol. Since the neutral complex 6 (Figure 7) is the most stable structure among its isomers (see the Figure S9 in SI15), possible pathways for the dehydrogenation of methanol with 6 were also calculated. As shown in Table S8 in SI15, the barriers for possible pathways for the dehydrogenation of methanol with 6 are over 39 kcal/mol relative to 6 and CH₃OH. Therefore, the dehydrogenation of methanol by either of these neutral species, 3 or 6, is unfavorable.

3.2.3. Hydroxide Attack on Formaldehyde and Formation of Formate. The calculated pathway for the hydroxide attack on formaldehyde and formation of formate is shown in Figure 7. Here, 1'' first cleaves water over transition state TS4_{1w}, where additional water acts as a proton shuttle to assist this process. The IRC analysis of TS4_{1w} shows that it connects the reactants (1'' + (H₂O···H₂O)) and the product complex (Int3). In TS4_{1w} (Figure 8), although a proton of the mediator water is

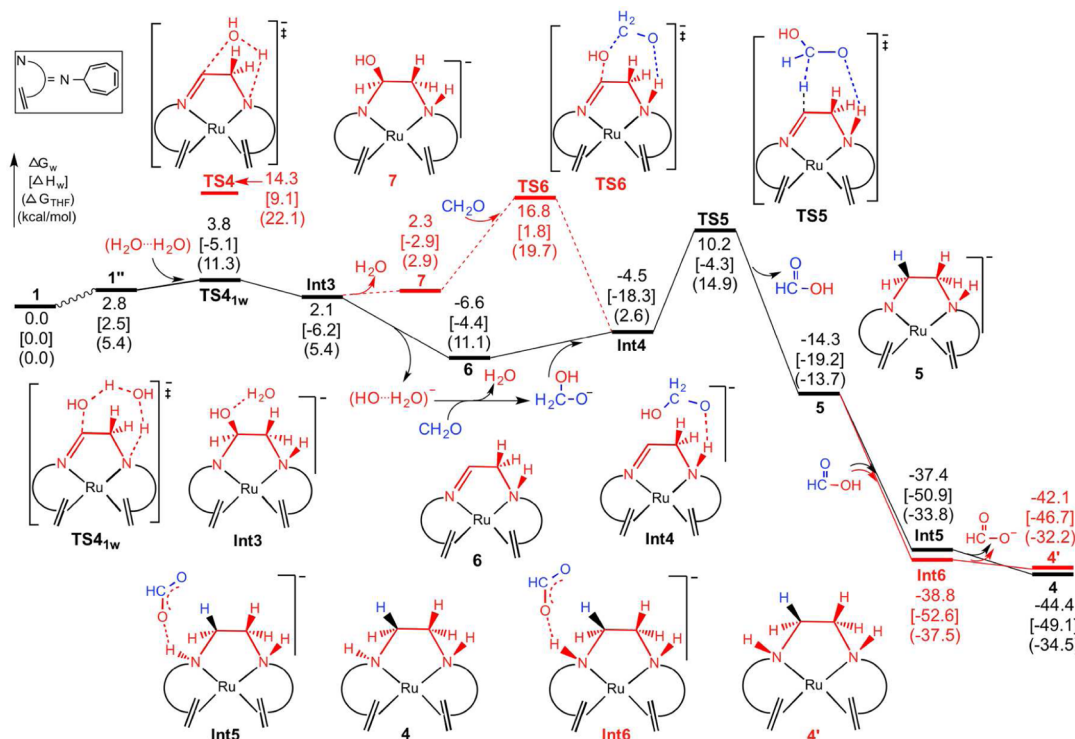


Figure 7. Energetic profiles for the hydroxide attack on formaldehyde and formation of formate.

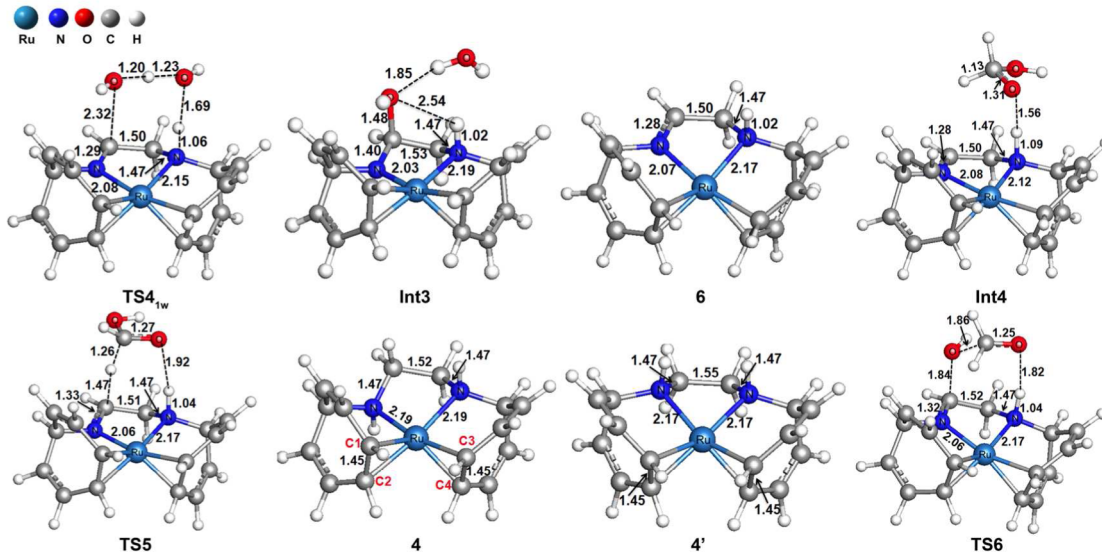


Figure 8. Optimized geometries for selected species in **Figure 7**. Geometries for the other species are in the Figure S26 in **SI15**. Selected bond distances (\AA) of the X-ray structure of **4_{exp}** are as follows: Ru–N: 2.121(2), C1/C3–C2/C4: 1.453(3).

almost on the nitrogen atom ($\text{N–H} = 1.06 \text{ \AA}$), the distance for the forming C–OH bond is 2.32 \AA , much longer (by 0.84 \AA) than that in the product **Int3**. The barrier for **TS4_{1w}** is only 3.8 kcal/mol relative to separated **1** and $(\text{H}_2\text{O}\cdots\text{H}_2\text{O})$, which is lower than that for the direct water cleavage transition state **TS4** by 10.5 kcal/mol . The formed intermediate **Int3**, which is at 2.1 kcal/mol , then dissociates $(\text{OH}\cdots\text{H}_2\text{O})^-$ to form a neutral intermediate **6**. Additional water molecules could further stabilize $(\text{OH}\cdots\text{H}_2\text{O})^-$; thus, we optimized **TS4_{1w}** in water at the level of M06/BS1/SMD(water), which converges to a transition state corresponding to a water's proton transferring to the N atom, forming **6** and $(\text{OH}\cdots\text{H}_2\text{O})^-$ directly. The barrier for this transition state is only 0.7 kcal/mol at the level of M06/BS2/SMD(water)//M06/BS1/SMD(water) relative to separated **1** and $(\text{H}_2\text{O}\cdots\text{H}_2\text{O})$. As shown in **Figure 7**, the formation of **6** and $(\text{OH}\cdots\text{H}_2\text{O})^-$ from **1** and $(\text{H}_2\text{O}\cdots\text{H}_2\text{O})$ is favorable in water ($\Delta G_w = -6.6 \text{ kcal/mol}$) but is less favorable in THF ($\Delta G_{\text{THF}} = 11.1 \text{ kcal/mol}$). The ΔG of this process is considered to be close to zero in the water–THF mixture (the reaction condition). Thus, the anionic species **1** and the neutral species **6** should easily interconvert based on the rapid equilibrium, $\text{1} + \text{H}_2\text{O} \rightleftharpoons \text{6} + \text{OH}^-$. In a proposed mechanism for the conversion of methanol and water to hydrogen and carbon dioxide by the anionic iridium complex, the conversion between anionic species and neutral species has been proposed on the basis of their experimental observations.^{5c}

Once the $(\text{OH}\cdots\text{H}_2\text{O})^-$ is released, it reacts rapidly with formaldehyde to yield a $\text{H}_2\text{C}(\text{OH})\text{O}^-$ anion and H_2O . Then, the $\text{H}_2\text{C}(\text{OH})\text{O}^-$ associates with **6** by forming a hydrogen bond to give intermediate **Int4**. Subsequently, the $\text{H}_2\text{C}(\text{OH})\text{O}$ group in **Int4** eliminates one H atom (on the C atom) to the ligand's carbon atom over transition state **TS5**, which is 14.7 kcal/mol above intermediate **Int4**. **Int4** and **TS5** are stabilized by hydrogen bond interactions at 1.56 and 1.92 \AA , respectively (**Figure 8**). In **TS5**, a H atom on the C atom of the $\text{H}_2\text{C}(\text{OH})\text{O}$ group is transferring to the ligand's C atom. The breaking C–H bond and the forming C–H bond are at 1.26 and 1.47 \AA , respectively, and the hydrogen bond weakens as the C=O bond forms. After **TS5**, the generated formic acid and **5**

are thermodynamically favored both in water ($\Delta G_w = -14.3 \text{ kcal/mol}$) and in THF ($\Delta G_{\text{THF}} = -13.7 \text{ kcal/mol}$). The formic acid then protonates complex **5** easily and leads directly to complexes **Int5** or **Int6**, which upon dissociation of HCOO^- lead to **4** or **4'**, respectively. The two protons on the N atoms are trans in **Int5** and **4** and cis in **Int6** and **4'**. Relative to separated reactants, **4** and **4'** are at -44.4 and -42.1 kcal/mol , respectively. Consistent with the experimental observation, species **4** with trans protonated Ns are 2.3 kcal/mol more stable than **4'** with cis protonated Ns. The optimized geometry of **4** in **Figure 8** is close to the X-ray crystal structure of **4_{exp}**.⁶ Computed structures for the actual catalyst system **4_{exp}** and its aldehyde complexes are shown in **SI16**. Although the metal–ligand interactions in **4'** (the Ru–N bond is at 2.17 \AA) are stronger than those in **4** (the Ru–N bond is at 2.19 \AA), the ligand frozen as in complex **4'** is less stable than that frozen as in complex **4** by 5.9 kcal/mol in electronic energy, as obtained by the single-point calculations at the level of M06/BS1.

An alternative pathway from **Int3** involves the dissociation of water to form an intermediate **7**, which is at 2.3 kcal/mol and then reacts with formaldehyde through transition state **TS6**, wherein the OH group of **7** adds to formaldehyde to form $\text{H}_2\text{C}(\text{OH})\text{O}$. A hydrogen bond interaction (1.82 \AA) is found in **TS6**, and the transferring OH group lies nearly equidistant from the two carbon atoms (**Figure 8**). **TS6**, which is 16.8 kcal/mol above the separate reactants, leads to intermediate **Int4** that then crosses transition state **TS5** to form **5** and formic acid. However, this pathway via **TS6** is less favorable than the pathway via **6**. In addition, the continuous consumption of OH^- by CH_2O drives the equilibrium ($\text{1} + \text{H}_2\text{O} \rightleftharpoons \text{6} + \text{OH}^-$) forward toward **6**.

It is known that methanediol $\text{H}_2\text{C}(\text{OH})_2$ can be formed directly from formaldehyde and water. Thus, possible mechanisms for the formation of methanediol, involving the direct coupling of formaldehyde and water, or catalyzed by one or two water molecules, or catalyzed by formic acid, were investigated (see **SI17**). Among them, the formic acid catalyzed transition state (at 14.6 kcal/mol) is the lowest one, but it is still less favorable than the pathway via **6**. Moreover, formic acid is a short-lived intermediate in the reaction. Once the

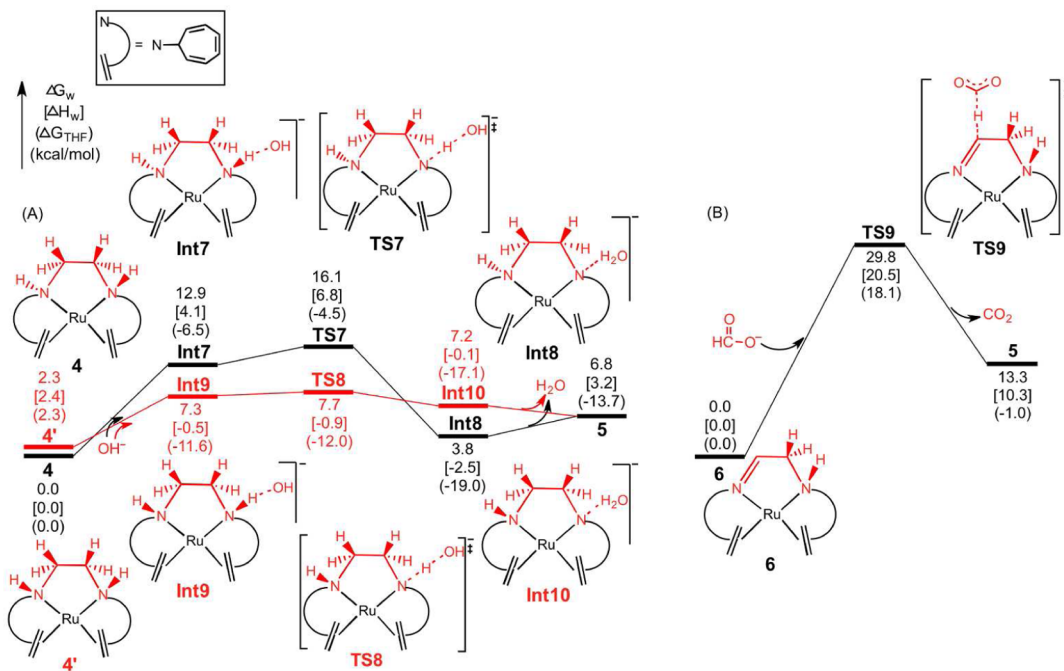


Figure 9. (A) Energetic profiles for the deprotonation of complexes **4** and **4'** relative to **4** and OH^- ; (B) energetic profiles for the decomposition of formate to form CO_2 relative to **6** and HCOO^- .

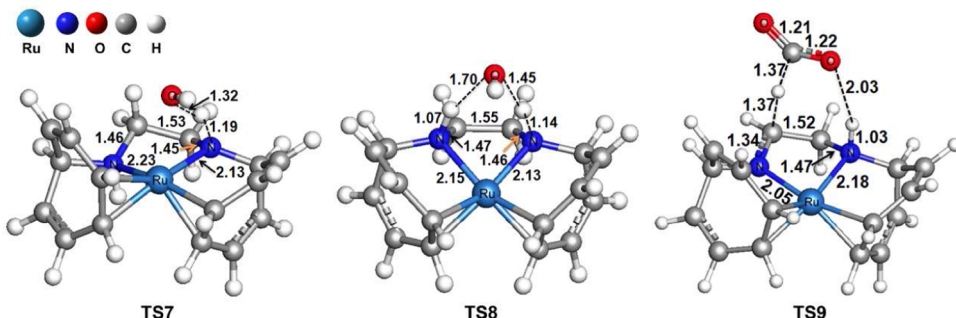


Figure 10. Optimized geometries for selected species in Figure 9. Geometries for the other species are in Figure S27 in SI15. Selected bond lengths are in Å.

methanediol is formed, it may react with the species **1''** by transferring its proton to the nitrogen atom in **1''** to form the intermediate **Int4** that then produces HCOOH by crossing **TSS**.

3.2.4. Hydride Transfer To Release Carbon Dioxide and Regenerate the Catalyst. Although complexes **4** and **4'** as shown in Figure 7 have high stability, they are easily deprotonated by OH^- to reform **5** again (Figure 9A). As discussed above, OH^- can be generated from the catalyst and water based on the equilibrium $\mathbf{1} + \text{H}_2\text{O} \rightleftharpoons \mathbf{6} + \text{OH}^-$. The process in Figure 9, panel A has low barriers, **TS7** at 16.1 kcal/mol and **TS8** at 5.4 kcal/mol relative to **4** and **4'**, respectively. An additional water, that is, by forming $(\text{OH}\cdots\text{H}_2\text{O})^-$, has little effect on this process (see SI8). The formations of **5** and H_2O are respectively 6.8 and -13.7 kcal/mol in water and in THF relative to **4** and OH^- . Thus, under the reaction conditions (the water–THF mixture), the transformation between the neutral species **4** and the anionic species **5** may also be in rapid equilibrium, $\mathbf{4} + \text{OH}^- \rightleftharpoons \mathbf{5} + \text{H}_2\text{O}$.

Consistent with Grützmacher and co-workers' experiments,⁴ **4** is very stable in THF,⁶ and the release of H_2 from **4** or its

isomers is computed to be unlikely, as the barriers for possible H_2 -release transition states are over 55 kcal/mol relative to **4** (see SI9). Thus, in one experiment,⁶ base ($\text{KO}^\ddagger\text{Bu}$) is employed to regenerate the catalyst **1** from **4**. The mechanism for this process was investigated (see SI10) where **4** deprotonates under base to form the species **5** that then releases H_2 to regenerate the catalyst **1**.

In a separate step, the neutral ruthenium complex **6** accepts a hydride from HCOO^- through **TS9** to produce CO_2 and **5** (Figure 9B). The barrier for **TS9** is 29.8 kcal/mol (in water) and is 18.1 kcal/mol (in THF) relative to separated **6** and HCOO^- . Therefore, the irreversible release of CO_2 (from HCOO^-) and H_2 (from **5**) drives the reaction forward. An alternative pathway, which involves the isomerization of the neutral complex **6** to its isomer in which two cis hydrogen atoms are on the ruthenium and nitrogen atoms, followed by the release of H_2 to generate **3** is computed to be less favorable (see SI11). In the Grützmacher and co-workers' experiment,⁶ reaction of EtOH and H_2O in a solution of **1** forms **4** and acetate. This reaction is proposed to proceed via a similar mechanism, involving dehydrogenation of EtOH to form

CH_3CHO , followed by the formation of CH_3COO^- and 4. However, CH_3COO^- could not be decomposed by the neutral complex 6 due to the lack of hydride atoms on the α -C. Thus, CH_3COO^- and 4 were observed in the experiment.

Optimized geometries of transition states TS7 and TS8 in Figure 10 correspond to the proton migrating from N atoms to OH^- . The distance between the migrating proton and the N atom in TS8 is shorter (by 0.05 Å) than that in TS7. In addition, a hydrogen-bond interaction at 1.70 Å in TS8 could stabilize its structure. Thus, TS8 is lower in energy than TS7. In TS9, the formate's hydrogen atom is transferring to the ligand's carbon atom, and the transferring H atom lies equidistant from the two carbon atoms. A hydrogen-bond interaction (at 2.03 Å) further stabilizes TS9.

An alternative pathway wherein 4 or 4' reacts with HCOO^- to release CO_2 and H_2 directly with formation of complex 5 was calculated. However, these barriers are very high (over 50 kcal/mol in water and over 37 kcal/mol in THF, see SI12). In addition, another alternative pathway involving ruthenium hydride complexes formed from 4 or 4' by accepting the hydride from HCOO^- (with the release of CO_2) is also unfavorable; the barriers for the release of H_2 from the formed ruthenium hydride complexes are over 50 kcal/mol in water and over 37 kcal/mol in THF, respectively (see SI12). Thus, these two possibilities are unlikely.

Experimentally, species 1 catalyzes formic acid's decomposition into CO_2 and H_2 in several minutes in 1,4-dioxane at 90 °C.⁶ Thus, any formic acid will decompose fairly rapidly; the energetic profile is shown in Figure 11. In this pathway, once 1"

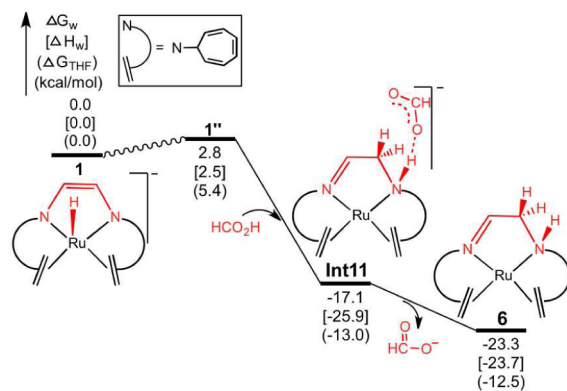


Figure 11. Energetic profiles for the decomposition of formic acid by catalyst 1. Optimized geometries for the species are in Figure S28 in SI15.

is formed via the hydrogen “walking” process, the formic acid protonates 1'' without any transition state to form intermediate Int11, followed by releasing HCOO^- to produce the neutral ruthenium complex 6. Subsequently, the neutral ruthenium complex 6 reacts with HCOO^- through TS9 to produce CO_2 and 5. The energetic profile in 1,4-dioxane ($\epsilon = 2.2099$) is assumed to be close to that in THF ($\epsilon = 7.4257$) in which the barrier for TS9 is 18.1 kcal/mol relative to 6 and HCOO^- .

In a previously reported production of acid from alcohol and water by transition metal complexes, the metal–acid complexes were observed without adding any base.⁵⁰ Thus, the base is required to regenerate the catalyst by releasing the carboxylate anion; the details have been investigated by DFT calculations.³³ In contrast, this reaction was reported to occur under neutral conditions. Thus, possible formic acid–ruthenium complexes

were investigated (see SI13). Among these complexes, the most stable one, which is an isomer of Int11 formed by adding the formic acid's O–H bond to the Ru–N bond of 1'' in which HCOO^- forms a Ru–O bond with the ruthenium atom, is −12.0 and −7.1 kcal/mol in water and THF, respectively, relative to separated catalyst 1 and formic acid. This isomer is less stable than Int11; thus, no stable metal–acid complexes are formed in this reaction.

To regenerate the catalyst 1, the complex 5 formed in the reaction must release H_2 . The calculated energy profiles for this process are shown in Figure 12, panel A, where complex 5 is

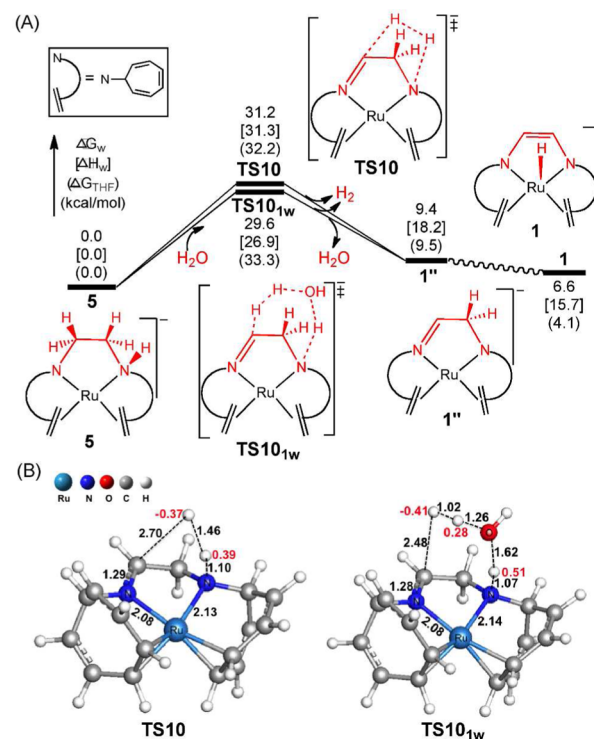


Figure 12. (A) Energetic profiles for the release of H_2 from the ruthenium complex 5. (B) Optimized geometries for the transition states TS10 and TS10_{1w}. Selected bond lengths are in Å, and red numbers on atoms are the NPA charges.

the energy reference. Two pathways were calculated: one is through a transition state TS10, where H_2 releases directly, and the other one is over transition state TS10_{1w}, where a water molecule mediates the release of H_2 . Optimizations by following the forward and backward directions of the imaginary frequencies of TS10 and TS10_{1w} converge to their products and reactants, respectively. Their barriers are close, 31.2 kcal/mol for TS10 and 29.6 kcal/mol for TS10_{1w}. As shown by their optimized geometries in Figure 12, panel B, water acts as a proton shuttle in TS10_{1w}, where the distance between the forming H–H bond is 1.02 Å, which is shorter than that in TS10 (1.46 Å). The distances for the breaking C–H bonds in both TS10 and TS10_{1w} are very long, 2.70 and 2.48 Å, respectively. This implies that the release of H_2 occurs asynchronously, where the C–H bond's hydrogen atom dissociates first, becoming hydride-like (see the NPA charges in their optimized geometries), which then withdraws the proton from the nitrogen atom or water to form H_2 . Since TS10_{1w} is lower in energy than TS10, we optimized TS10_{1w} in water at the level of M06/BS1/SMD(water), which converges

to a transition state for the H₂ release with the formation of OH⁻ and **6**; the barrier for this transition state is 26.8 kcal/mol at the level of M06/BS2/SMD(water)//M06/BS1/SMD-(water) relative to separated **5** and H₂O. One would expect additional water molecules would further stabilize this transition state. The equilibrium between **6** and **1**, $\mathbf{6} + \text{OH}^- \rightleftharpoons \mathbf{1} + \text{H}_2\text{O}$, then transforms OH⁻ and **6** back to **1** and H₂O. After H₂ is released, **1''** is formed, followed by the isomerization to regenerate the catalyst **1**. Although the formation of **1** and H₂ from **5** is endergonic by 6.6 kcal/mol, this process is irreversible due to the release of H₂, thereby driving the reaction forward. Other possible mechanisms for the release of H₂ from **5** or its isomers were investigated (see SI14). However, these possibilities are unfavorable because the transition states for these mechanisms are higher than **TS10_{1w}**.

3.3. Results for the Actual Catalyst. Total catalytic cycles for the reaction of CH₃OH and H₂O to form CO₂ and H₂ catalyzed by **1** are shown in Figure 13. Catalyst **1** is involved in

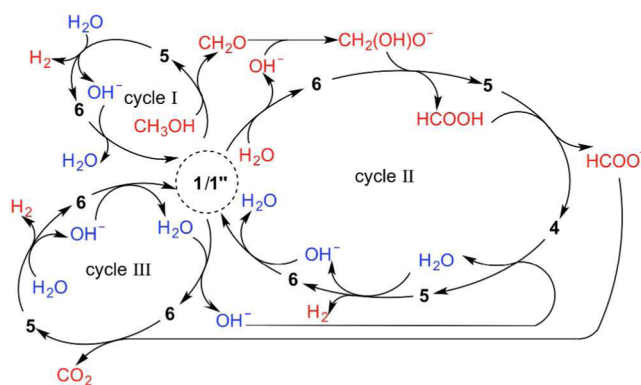


Figure 13. Total catalytic cycles for the reaction of CH₃OH and H₂O to form CO₂ and H₂ catalyzed by **1**. Reactants and their transformed species are shown in red, and the mediator H₂O and its transformed species OH⁻ are shown in blue.

the three cycles: dehydrogenation of CH₃OH to form CH₂O with releasing one H₂ (cycle I), OH⁻ attack on CH₂O and formation of formate with releasing another H₂ (cycle II), and hydride transfer to release CO₂ and regenerate the catalyst with releasing the third H₂ (cycle III). By using the mechanism predicted for the catalyst model **1**, key transition states and intermediates involved in the catalytic mechanism for the actual catalyst, **1_exp**, were recalculated. The energetic results are shown in Table 1. **TS1_exp** is very close to **TS1** in energy. The relative energies for **X_exp** are higher than those for **X** in the hydrogen “walking” process, dehydrogenation of methanol to formaldehyde, hydroxide attack on formaldehyde and formation of formate, and regenerate the catalyst (in Table 1, “X” denotes species number corresponding to the two complexes, model ligand vs full ligand). Furthermore, in the deprotonation of complex **4_exp** and the hydride transfer to release carbon dioxide, the energies for **X_exp** are lower than those for **X**. Although the energy differences between **X_exp** and **X** vary by several kcal/mol, the comparisons show that it is reasonable to simplify the actual catalyst **1_exp** to **1** because the mechanism does not change. The release of H₂ over **TS10_{1w}_exp** is also the rate-determining step, in agreement with that for the model system. Moreover, the direct H₂-release transition state **TS10_exp** is higher by 6.3 kcal/mol than the water-assisted H₂-release transition state **TS10_{1w}_exp**. Relative

to separated **5_exp** and H₂O, the barrier for **TS10_{1w}_exp** is high, 34.9 kcal/mol in water and 38.4 kcal/mol in THF, respectively. However, the release of H₂ under reflux and the high reaction temperature (90 °C) is considered sufficient to drive the reaction forward.

The influence of functionals was examined here by calculating the rate-determining transition state **TS10_{1w}_exp** (the release of hydrogen from the complex **5_exp**) with five functionals selected from SI1. Among them, the M06L functional gives the lowest barrier for **TS10_{1w}_exp**, which is 32.4 kcal/mol. The ωB97XD functional produces the results that are very close to those for the M06 functional. The other functionals predict the barriers for **TS10_{1w}_exp** that are higher by several kcal/mol than that from the M06 functional. Although it is unclear which functional predicts results that are closest to the experiment, the high barriers (more than 30 kcal/mol) for the rate-determining step (the release of H₂ from **5_exp**) are consistent with reaction conditions reported in the experiment.

4. CONCLUSION

In summary, DFT calculations with the M06 functional were conducted to investigate the mechanism for the production of carbon dioxide and hydrogen from methanol and water catalyzed by the anionic ruthenium complex **1_exp** with a chemically non-innocent ligand. In the literature, a neutral ruthenium complex **3_exp** formed from the reaction of **1_exp** and water with the release of hydrogen was proposed to catalyze the reaction. The electronic structures of the anionic ruthenium complex **1** and its isomers were analyzed by NBO calculations, and the nature of their non-innocent ligands was elucidated. Our investigations show that the reaction mechanism catalyzed by the anion, **1**, is more favorable than that catalyzed by the neutral, **3**. In the catalytic mechanism by **1**, the intermediate **1''** formed from **1** through migration of the hydrogen atom from the ruthenium to the meta-carbon atom in the ligand is an important species. In **1''**, the C atom of the –CH=N– bond and the N atom of the –CH₂–N= bond in the ligand construct an active site for the catalysis. When H migrates from Ru to C, a frustrated Lewis pair (FLP) is generated in the ring between N and C. The computed catalytic mechanism involves three steps: dehydrogenation of methanol to formaldehyde, hydroxide attack on formaldehyde and formation of formate, and hydride transfer to release carbon dioxide and regenerate the catalyst. The dehydrogenation of methanol occurs on the ligand of **1''**, where two hydrogen atoms (one on the O atom and the other one on the C atom) simultaneously move to the ligand’s nitrogen and carbon atoms (the FLP), respectively, forming complex **5**. In the process for hydroxide attack on formaldehyde and formation of formate, the catalyst first cleaves water, followed by the dissociation of OH⁻ to form a neutral complex **6**, building on the equilibrium of $\mathbf{1} + \text{H}_2\text{O} \rightleftharpoons \mathbf{6} + \text{OH}^-$ under the reaction conditions. The generated OH⁻ reacts with formaldehyde immediately to form a H₂C(OH)O⁻ anion. Subsequently, a hydride of H₂C(OH)O⁻ moves to the ligand’s C atom of **6** to give formic acid and **5**. The formic acid then protonates **5** easily to generate complex **4** or **4'**, which are considered as stable resting states in the reaction. **4** or **4'** is found to be deprotonated by the formed OH⁻ to reform **5** again, resulting from the equilibrium, $\mathbf{4} + \text{OH}^- \rightleftharpoons \mathbf{5} + \text{H}_2\text{O}$. In addition, the formed neutral complex **6** is computed to assist the decomposition of formate to release CO₂ by transferring the hydride of formate to the sp² C atom of

Table 1. Results for Some Transition States and Intermediates for the Actual Catalyst System and the Corresponding Model System in Italic. Energies in kcal/mol Are $\Delta G_w[\Delta H_w](\Delta G_{\text{THF}})$ ^a

| hydrogen “walking” process | | | | |
|--------------------------------------------------------------------------------------------------------|------------------------------------------------------------------------------------|---------------------------------------------------------------------------------------------------------------|--------------------------------------------------------------------------|------------------------------------------------------------------------------------------------|
| relative to the catalyst 1_exp and ($\text{H}_2\text{O}\cdots\text{H}_2\text{O}$) | TS1_exp 19.3[18.9](19.1) 19.3[18.3](18.9) | 1'_exp 9.2[9.3](9.1) 6.5[6.7](5.9) | TS2_w_exp 16.6[9.6](17.6) 12.8[5.4](17.6) | 1''_exp 3.4[3.6](6.1) 2.8[2.5](5.4) |
| | | | dehydrogenation of methanol to formaldehyde | |
| relative to 1_exp and CH_3OH | | TS3_exp 27.4[15.9](34.2) 23.8[13.2](30.0) | | 5_exp + CH₂O 12.2[11.9](9.9) 11.3[10.5](9.9) |
| hydroxide attack on formaldehyde and formation of formate | | | | |
| relative to 1_exp , ($\text{H}_2\text{O}\cdots\text{H}_2\text{O}$), and CH_2O | TS4_{1w}_exp + CH₂O 7.9[0.2](10.9) 3.8[-5.1](11.3) | 6_exp + (OH\cdots H₂O)⁻ + CH₂O -1.1[1.5](13.3) -6.6[-4.4](11.1) | Int4_exp + H₂O 2.2[-11.1](10.0) -4.5[-18.3](2.6) | TS5_exp + H₂O 13.1[-1.1](18.4) 10.2[-4.3](14.9) |
| | | | | 4_exp + HCOO⁻ + H₂O -38.6[-43.5](−28.3) -44.4[-49.1](−34.5) |
| deprotonation of complex 4_exp | | | | |
| relative to 4_exp and OH^- | | 4'_exp + OH⁻ 1.8[2.2](2.0) 2.3[2.4](2.3) | TS7_exp 12.2[3.5](−10.2) 16.1[6.8](−4.5) | 5_exp + H₂O 1.9[-1.0](−23.7) 6.8[3.2](−13.7) |
| hydride transfer to release carbon dioxide | | | | |
| relative to 6_exp and HCOO^- | TS9_exp 25.7[16.2](15.9) 29.8[20.5](18.1) | 5_exp + CO₂ 8.7[5.9](−6.4) 13.3[10.3](−1.0) | relative to 5_exp and H_2O | TS10_exp 41.2[41.0](41.5) 31.2[31.3](32.2) |
| | | | | TS10_{1w}_exp 34.9[31.0](38.4) 29.6[26.9](33.3) |
| | | | | regenerate the catalyst |

^aOptimized geometries for the species are in Figure S29 in [SI15](#).**Table 2.** Results for **TS10_{1w}_exp** for the Release of Hydrogen with Different Functionals^a

| functionals | TS10_{1w}_exp |
|----------------|------------------------------|
| ω B97XD | 34.9[31.4](38.1) |
| M06L | 32.4[28.7](36.1) |
| CAM-B3LYP | 36.0[32.2](38.6) |
| OHSE2PBE | 38.3[34.3](41.3) |
| MN12SX | 40.8[37.0](43.5) |

^aEnergies in kcal/mol are $\Delta G_w[\Delta H_w](\Delta G_{\text{THF}})$ relative to separated **5_exp** and water.

6, leading to **5**. Finally, complex **5** releases H_2 to regenerate the catalyst. The release of CO_2 (from formate) and H_2 (from **5**) is irreversible, which is considered to drive the reaction forward. Although the energies for selected transition states and intermediates for the actual catalyst system with the full ligands vary in several kcal/mol in comparison to that for the model system, the catalytic mechanisms for both systems are the same. The release of hydrogen is still the rate-determining step in the actual catalyst system; the barrier is over 30 kcal/mol with a variety of different functionals. The release of H_2 and the high reaction temperature (90 °C) drives the reaction forward.

In the studied mechanism, the whole reaction occurs on the chemically non-innocent ligand with the ruthenium atom appearing as a spectator. This is unusual because, traditionally, reactions by transition metal complexes have been found to occur on the metal center with the ligands as spectators. The reaction looks like an organic reaction, as the Ru center does not participate directly in the reaction. The ligand-based mechanism proposed here provides a direction to design new catalysts by replacing the Ru atom with other metal atoms, for example, a less costly, benign iron atom, or with nonmetal atoms (an extension of transition metal catalysis to organic catalysis). Furthermore, this study suggests the possibility of the

ligand-based mechanisms for other transition-metal-catalyzed reactions.

ASSOCIATED CONTENT

Supporting Information

The Supporting Information is available free of charge on the ACS Publications website at DOI: [10.1021/jacs.5b07444](https://doi.org/10.1021/jacs.5b07444).

Benchmark calculation results; adjustments for the standard-state concentration; NBO results for species **1**, **1'**, and **1''**; other pathways for hydrogen “walking” process; other pathways for the dehydrogenation of methanol; **4_exp** and its aldehyde complexes; formation of methanediol; deprotonation of complex **4** or **4'** by $(\text{OH}\cdots\text{H}_2\text{O})^-$; release of H_2 from the neutral complex **4**; regeneration of the catalyst **1** from **4** with $\text{KO}^\ddagger\text{Bu}$; release of H_2 from the neutral complex **6**; alternative pathways for the release of CO_2 from formate; possible formic acid–ruthenium complexes; unfavorable mechanism for the release of hydrogen; optimized geometries for the species in the text; Cartesian coordinates of the species in the text and their absolute energies ([PDF](#)).

AUTHOR INFORMATION

Corresponding Author

*mbhall@tamu.edu

Notes

The authors declare no competing financial interest.

ACKNOWLEDGMENTS

This work was funded by the National Science Foundation (CHE-1300787) and by the Welch Foundation (A-0648). Texas A&M Supercomputing Facility was acknowledged to provide computing resources. We thank Professor Grützmacher for discussions on the mechanism.

■ REFERENCES

- (1) Olah, G. A.; Prakash, G. K. S.; Goepert, A. *J. Am. Chem. Soc.* **2011**, *133*, 12881–12898.
- (2) Palo, D. R.; Dagle, R. A.; Holladay, J. D. *Chem. Rev.* **2007**, *107*, 3992–4021.
- (3) (a) Cortright, R. D.; Davda, R. R.; Dumesic, J. A. *Nature* **2002**, *418*, 964–967. (b) Shabaker, J. W.; Davda, R. R.; Huber, G. W.; Cortright, R. D.; Dumesic, J. A. *J. Catal.* **2003**, *215*, 344–352.
- (4) (a) Daresbourg, D. J.; Holtcamp, M. W. *Coord. Chem. Rev.* **1996**, *153*, 155–174. (b) Leitner, W. *Coord. Chem. Rev.* **1996**, *153*, 257–284. (c) Sakakura, T.; Choi, J.-C.; Yasuda, H. *Chem. Rev.* **2007**, *107*, 2365–2387. (d) Daresbourg, D. J. *Inorg. Chem.* **2010**, *49*, 10765–10780. (e) Mikkelsen, M.; Jørgensen, M.; Krebs, F. C. *Energy Environ. Sci.* **2010**, *3*, 43–81. (f) Aresta, M. *Activation of Small Molecules*; Tolman, W. B., Ed.; Wiley-VCH: Weinheim, Germany, 2010. (g) Behr, A.; Henze, G. *Green Chem.* **2011**, *13*, 25–39. (h) Yang, Z.-Z.; He, L.-N.; Gao, J.; Liu, A.-H.; Yu, B. *Energy Environ. Sci.* **2012**, *5*, 6602–6639. (i) Dibenedetto, A.; Angelini, A.; Stufano, P. *J. Chem. Technol. Biotechnol.* **2014**, *89*, 334–353.
- (5) (a) Nielsen, M.; Alberico, E.; Baumann, W.; Drexler, H.-J.; Junge, H.; Gladiali, S.; Beller, M. *Nature* **2013**, *495*, 85–89. (b) Hu, P.; Diskin-Posner, Y.; Ben-David, Y.; Milstein, D. *ACS Catal.* **2014**, *4*, 2649–2652. (c) Fujita, K.-i.; Kawahara, R.; Aikawa, T.; Yamaguchi, R. *Angew. Chem., Int. Ed.* **2015**, *54*, 9057–9060.
- (6) Rodríguez-Lugo, R. E.; Trincado, M.; Vogt, M.; Tewes, F.; Santiso-Quinones, G.; Grützmacher, H. *Nat. Chem.* **2013**, *5*, 342–347.
- (7) Monney, A.; Barsch, E.; Sponholz, P.; Junge, H.; Ludwig, R.; Beller, M. *Chem. Commun.* **2014**, *50*, 707–709.
- (8) (a) Yang, X. *ACS Catal.* **2014**, *4*, 1129–1133. (b) Lei, M.; Pan, Y.; Ma, X. *Eur. J. Inorg. Chem.* **2015**, *2015*, 794–803.
- (9) Breher, F.; Böhler, C.; Frison, G.; Harmer, J.; Liesum, L.; Schweiger, A.; Grützmacher, H. *Chem. - Eur. J.* **2003**, *9*, 3859–3866.
- (10) Luca, O. R.; Crabtree, R. H. *Chem. Soc. Rev.* **2013**, *42*, 1440–1459.
- (11) Tsurugi, H.; Saito, T.; Tanahashi, H.; Arnold, J.; Mashima, K. *J. Am. Chem. Soc.* **2011**, *133*, 18673–18683.
- (12) Caulton, K. G. *Eur. J. Inorg. Chem.* **2012**, *2012*, 435–443.
- (13) Greulich, S.; Klein, A.; Knodler, A.; Kaim, W. *Organometallics* **2002**, *21*, 765–769.
- (14) De Bruin, B.; Hetterscheid, D. G. H. *Eur. J. Inorg. Chem.* **2007**, *2007*, 211–230.
- (15) (a) Hehre, W. J.; Ditchfie, R.; Pople, J. A. *J. Chem. Phys.* **1972**, *56*, 2257–2261. (b) Franci, M. M.; Pietro, W. J.; Hehre, W. J.; Binkley, J. S.; Gordon, M. S.; Defrees, D. J.; Pople, J. A. *J. Chem. Phys.* **1982**, *77*, 3654–3665.
- (16) (a) McLean, A. D.; Chandler, G. S. *J. Chem. Phys.* **1980**, *72*, 5639–5648. (b) Krishnan, R.; Binkley, J. S.; Seeger, R.; Pople, J. A. *J. Chem. Phys.* **1980**, *72*, 650–654.
- (17) Clark, T.; Chandrasekhar, J.; Spitznagel, G. W.; Schleyer, P. v. R. *J. Comput. Chem.* **1983**, *4*, 294–301.
- (18) Andrae, D.; Häussermann, U.; Dolg, M.; Stoll, H.; Preuss, H. *Theor. Chem. Acc.* **1990**, *77*, 123–141.
- (19) Dunning, T. H. *J. Chem. Phys.* **1989**, *90*, 1007–1023.
- (20) (a) Feller, D. *J. Comput. Chem.* **1996**, *17*, 1571–1586. (b) Schuchardt, K. L.; Didier, B. T.; Elsethagen, T.; Sun, L.; Gurumoorthi, V.; Chase, J.; Li, J.; Windus, T. L. *J. Chem. Inf. Model.* **2007**, *47*, 1045–1052.
- (21) Zhao, Y.; Truhlar, D. G. *J. Chem. Phys.* **2006**, *125*, 194101.
- (22) Zhao, Y.; Truhlar, D. G. *Theor. Chem. Acc.* **2008**, *120*, 215–241.
- (23) Peverati, R.; Truhlar, D. G. *J. Chem. Phys.* **2011**, *135*, 191102.
- (24) (a) Perdew, J. P.; Ernzerhof, M.; Burke, K. *J. Chem. Phys.* **1996**, *105*, 9982–9985. (b) Adamo, C.; Barone, V. *J. Chem. Phys.* **1999**, *110*, 6158–6170.
- (25) Austin, A.; Petersson, G. A.; Frisch, M. J.; Dobek, F. J.; Scalmani, G.; Throssell, K. *J. Chem. Theory Comput.* **2012**, *8*, 4989–5007.
- (26) Chai, J.-D.; Head-Gordon, M. *Phys. Chem. Chem. Phys.* **2008**, *10*, 6615–6620.
- (27) Yanai, T.; Tew, D. P.; Handy, N. C. *Chem. Phys. Lett.* **2004**, *393*, 51–57.
- (28) (a) Heyd, J.; Scuseria, G. E. *J. Chem. Phys.* **2004**, *121*, 1187–1192. (b) Heyd, J.; Scuseria, G. E. *J. Chem. Phys.* **2004**, *120*, 7274–7280.
- (29) Peverati, R.; Truhlar, D. G. *Phys. Chem. Chem. Phys.* **2012**, *14*, 16187–16191.
- (30) Purvis, G. D., III; Bartlett, R. J. *J. Chem. Phys.* **1982**, *76*, 1910–1918.
- (31) Pople, J. A.; Head-Gordon, M.; Raghavachari, K. *J. Chem. Phys.* **1987**, *87*, 5968–5975.
- (32) Gusev, D. G. *Organometallics* **2013**, *32*, 4239–4243.
- (33) Li, H.; Hall, M. B. *J. Am. Chem. Soc.* **2014**, *136*, 383–395.
- (34) Fukui, K. *Acc. Chem. Res.* **1981**, *14*, 363–368.
- (35) Marenich, A. V.; Cramer, C. J.; Truhlar, D. G. *J. Phys. Chem. B* **2009**, *113*, 6378–6396.
- (36) (a) Cramer, C. J. *Essentials of Computational Chemistry: Theories and Models*, 2nd ed.; John Wiley & Sons, Ltd: New York, 2004; pp 378–379. (b) Vigara, L.; Ertem, M. Z.; Planas, N.; Bozoglian, F.; Leidel, N.; Dau, H.; Haumann, M.; Gagliardi, L.; Cramer, C. J.; Llobet, A. *Chem. Sci.* **2012**, *3*, 2576–2586.
- (37) (a) Webster, C. E.; Pérez, L. M.; Hall, M. B. *Jimp 2, version 091, 2006*. <http://www.chem.tamu.edu/jimp2/index.html>. (b) Hall, M. B.; Fenske, R. F. *Inorg. Chem.* **1972**, *11*, 768–775. (c) Bursten, B. E.; Jensen, J. R.; Fenske, R. F. *J. Chem. Phys.* **1978**, *68*, 3320–3321.
- (38) Frisch, M. J.; Trucks, G. W.; Schlegel, H. B.; Scuseria, G. E.; Robb, M. A.; Cheeseman, J. R.; Scalmani, G.; Barone, V.; Mennucci, B.; Petersson, G. A.; Nakatsuji, H.; Caricato, M.; Li, X.; Hratchian, H. P.; Izmaylov, A. F.; Bloino, J.; Zheng, G.; Sonnenberg, J. L.; Hada, M.; Ehara, M.; Toyota, K.; Fukuda, R.; Hasegawa, J.; Ishida, M.; Nakajima, T.; Honda, Y.; Kitao, O.; Nakai, H.; Vreven, T.; Montgomery, J. A., Jr.; Peralta, J. E.; Ogliaro, F.; Bearpark, M.; Heyd, J. J.; Brothers, E.; Kudin, K. N.; Staroverov, V. N.; Kobayashi, R.; Normand, J.; Raghavachari, K.; Rendell, A.; Burant, J. C.; Iyengar, S. S.; Tomasi, J.; Cossi, M.; Rega, N.; Millam, J. M.; Klene, M.; Knox, J. E.; Cross, J. B.; Bakken, V.; Adamo, C.; Jaramillo, J.; Gomperts, R.; Stratmann, R. E.; Yazyev, O.; Austin, A. J.; Cammi, R.; Pomelli, C.; Ochterski, J. W.; Martin, R. L.; Morokuma, K.; Zakrzewski, V. G.; Voth, G. A.; Salvador, P.; Dannenberg, J. J.; Dapprich, S.; Daniels, A. D.; Farkas, O.; Foresman, J. B.; Ortiz, J. V.; Cioslowski, J.; Fox, D. J. *Gaussian 09*, revision B.01; Gaussian, Inc.: Wallingford, CT, 2009.
- (39) (a) Werner, H.-J.; Knowles, P. J.; Knizia, G.; Manby, F. R.; Schütz, M. *WIREs Comput. Mol. Sci.* **2012**, *2*, 242–253. (b) Werner, H.-J.; Knowles, P. J.; Knizia, G.; Manby, F. R.; Schütz, M.; Celani, P.; Korona, T.; Lindh, R.; Mitrushenkov, A.; Rauhut, G.; Shamasundar, K. R.; Adler, T. B.; Amos, R. D.; Bernhardsson, A.; Berning, A.; Cooper, D. L.; Deegan, M. J. O.; Dobbyn, A. J.; Eckert, F.; Goll, E.; Hampel, C.; Hesselmann, A.; Hetzer, G.; Hrenar, T.; Jansen, G.; Köppel, C.; Liu, Y.; Lloyd, A. W.; Mata, R. A.; May, A. J.; McNicholas, S. J.; Meyer, W.; Mura, M. E.; Nicklass, A.; O'Neill, D. P.; Palmieri, P.; Peng, D.; Pflüger, K.; Pitzer, R.; Reiher, M.; Shiozaki, T.; Stoll, H.; Stone, A. J.; Tarroni, R.; Thorsteinsson, T.; Wang, M. *MOLPRO, version 2010.1, a Package of Ab Initio Programs*. <http://www.molpro.net>.
- (40) (a) Weinhold, F.; Landis, C. R. *Chem. Educ. Res. Pract.* **2001**, *2*, 91–104. (b) Weinhold, F.; Landis, C. R. *Discovering Chemistry with Natural Bond Orbitals*; John Wiley & Sons: Hoboken, NJ, 2012; pp 132–133.
- (41) Verendel, J. J.; Dinér, P. *ChemCatChem* **2013**, *5*, 2795–2797.
- (42) Alberico, E.; Sponholz, P.; Cordes, C.; Nielsen, M.; Drexler, H.-J.; Baumann, W.; Junge, H.; Beller, M. *Angew. Chem., Int. Ed.* **2013**, *52*, 14162–14166.
- (43) (a) Huang, F.; Lu, G.; Zhao, L.; Li, H.; Wang, Z.-X. *J. Am. Chem. Soc.* **2010**, *132*, 12388–12396. (b) Chakraborty, S.; Zhang, J.; Krause, J. A.; Guan, H. *J. Am. Chem. Soc.* **2010**, *132*, 8872–8873. (c) Huang, F.; Zhang, C.; Jiang, J.; Wang, Z.-X.; Guan, H. *Inorg. Chem.* **2011**, *50*, 3816–3825.
- (44) (a) Froese, R. D. J.; Jazdzewski, B. A.; Klosin, J.; Kuhlman, R. L.; Theriault, C. N.; Welsh, D. M.; Abboud, K. A. *Organometallics* **2011**, *30*, 251–262. (b) Kraft, S. J.; Williams, U. J.; Daly, S. R.; Schelter, E. J.; Kozimor, S. A.; Boland, K. S.; Kikkawa, J. M.; Forrest, W. P.; Christensen, C. N.; Schwarz, D. E.; Fanwick, P. E.; Clark, D. L.

- Conradson, S. D.; Bart, S. C. *Inorg. Chem.* **2011**, *50*, 9838–9848.
(c) Tsurugi, H.; Ohnishi, R.; Kaneko, H.; Panda, T. K.; Mashima, K. *Organometallics* **2009**, *28*, 680–687. (d) Kreisel, K. A.; Yap, G. P. A.; Theopold, K. H. *Eur. J. Inorg. Chem.* **2012**, *2012*, 520–529.
(45) Ng, S. M.; Zhao, C.; Lin, Z. Y. *J. Organomet. Chem.* **2002**, *662*, 120–129.
(46) Balcells, D.; Nova, A.; Clot, E.; Gnanamgari, D.; Crabtree, R. H.; Eisenstein, O. *Organometallics* **2008**, *27*, 2529–2535.
(47) Handgraaf, J.-W.; Reek, J. N. H.; Meijer, E. J. *Organometallics* **2003**, *22*, 3150–3157.
(48) (a) Li, H.; Hall, M. B. *ACS Catal.* **2015**, *5*, 1895–1913. (b) Li, H.; Wang, Z. *Sci. China: Chem.* **2012**, *55*, 1991–2008. (c) Li, H.; Wang, X.; Huang, F.; Lu, G.; Jiang, J.; Wang, Z.-X. *Organometallics* **2011**, *30*, 5233–5247. (d) Li, H.; Wang, X.; Wen, M.; Wang, Z.-X. *Eur. J. Inorg. Chem.* **2012**, *2012*, 5011–5020. (e) Qu, S.; Dang, Y.; Song, C.; Wen, M.; Huang, K.-W.; Wang, Z.-X. *J. Am. Chem. Soc.* **2014**, *136*, 4974–4991.
(49) Yamakawa, M.; Ito, H.; Noyori, R. *J. Am. Chem. Soc.* **2000**, *122*, 1466–1478.
(50) Balaraman, E.; Khaskin, E.; Leitus, G.; Milstein, D. *Nat. Chem.* **2013**, *5*, 122–125.